

Microstructure and Texture Evolution During the Alternate Extrusion of an AZ31 Magnesium Alloy

FENG LI,^{1,2} HONG WEI JIANG,¹ and YANG LIU¹

1.—School of Materials Science and Engineering, Harbin University of Science and Technology, Harbin 150040, People's Republic of China. 2.—e-mail: fli@hrbust.edu.cn

In this study, a new extrusion process, alternate extrusion (AE), is proposed. We evaluated the reliability and superiority of this process in practical applications by conducting a simulation using the finite element method, which confirmed the experimental results. The microstructure characteristics of an AZ31 magnesium alloy produced by conventional extrusion (CE) and AE were investigated by electron backscattered diffraction and optical microscopy, and the effects of the microstructures on the mechanical properties were studied across the extruded specimens. The main advantage of AE is that the load is reduced to less than half that in the CE process; this results from the reduced cross-section of the split punches. Additionally, the grain size with AE is more refined than with CE because of the additional shear force, which improves the mechanical properties of the alloys. Furthermore, AE can also weaken the intensity of the basal plane texture.

INTRODUCTION

Magnesium alloys have low densities, high specific strengths and good recycling characteristics, which means they are favored for energy saving, environmental protection, and other applications, particularly when light-weight materials are required.^{1–3} However, their hexagonal close-packed (HCP) structures mean that these materials have limited strength and ductility at room temperature.⁴ Grain refinement has proven to be an effective way to overcome these disadvantages.⁵ The metal is under a strong three-compressive stress state in the extrusion process, which can give full play to its plasticity. Therefore, the extrusion process is particularly suitable for the preparation of low-plasticity magnesium alloy.^{6,7} However, the capacity of conventional extrusion (CE) for grain refinement is limited. In recent years, the development of a fine-grained magnesium alloy extrusion process has been a focus area for research, and techniques such as equal channel angular press (ECAP),^{8–10} cyclic extrusion compression (CEC)¹¹ and accumulative back extrusion (ABE)¹² have been reported. These methods have developed rapidly. Kim et al.¹³ obtained a fine-grained structure using equal channel

angular extrusion (ECAE), which can effectively weaken the basal texture of the magnesium alloy material and at the same time control its texture. Xia et al.¹⁴ found that the grain size of AZ31 magnesium alloy could be considerably refined with ECAP, and after four passes at 150°C, or two passes at 100°C, the grain size could reach 1 μm. Wang et al.¹⁵ put forward C-shaped equal channel reciprocating extrusion (CECRE), which adopts the combination of CEC and ECAE. Four repetitions of CECRE increased the strain value to 11, and a uniform fine grain with an average size of about 3.6 μm was obtained. Fatemi-Varzaneh et al.¹⁶ found that AZ31 magnesium alloy could be successfully extruded by ABE. A uniform ultrafine grain size of 1 μm was obtained after four passes of ABE. Although these processes considerably refine the grains, the large friction is the main disadvantages of those methods for wider industrialization.

Based on such a background, we propose a fine-grained extrusion process called alternate extrusion (AE) and study the AZ31 magnesium alloy microstructure and texture distribution after the molding process. We found the load in this method reduced, the grain size refined and the intensities of basal plane texture weakened.

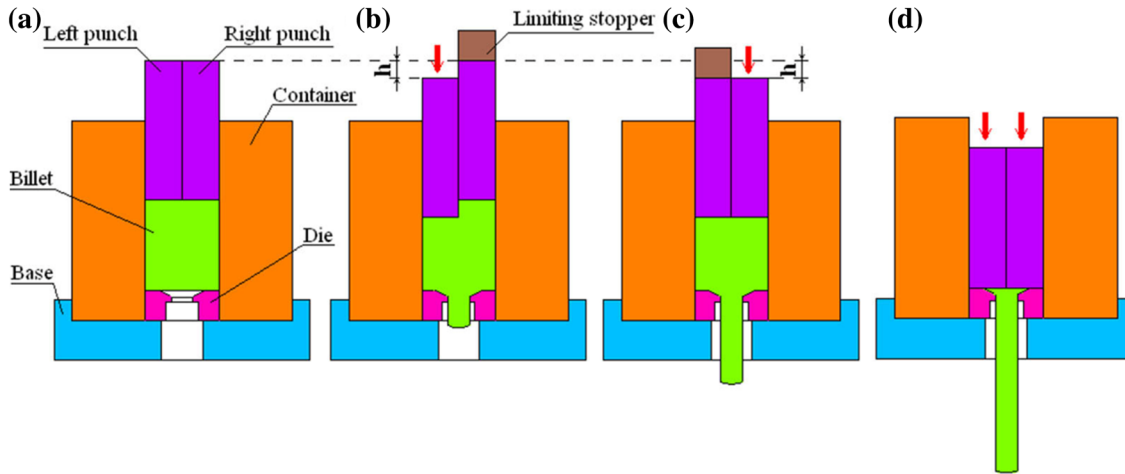


Fig. 1. Schematic AE process: (a) initial state, (b) left punch loading, (c) right punch loading, one cycle, and (d) end of process.

AE PROCESS PRINCIPLES

AE breaks through the traditional extrusion punch with the whole design concept, which uses two or more punches alternately loaded in the extrusion process. Compared with CE, the material both around the extrusion die and the axis portions of the billet are subjected to sustained severe shear deformation, which promotes the billet to refine during the extrusion process. Because split punches alternately apply downward loading, AE can significantly reduce the extrusion load within a single pass. The schematic AE process is shown in Fig. 1.

Figure 1 shows the CE process, in which two punches synchronously apply a downward load. At the beginning of the forming stage, the right punch is fixed with a limit device, and the left punch strokes down h ($h = 8$ mm). Then, the left punch is fixed and the right punch strokes down h . Following this loading pattern, downward loading is applied by alternating left and right punches until the extrusion billet is completely formed. Owing to the relatively small size of the billet used in this research, it was processed in three passes.

EXPERIMENTAL AND SIMULATION PROCEDURE

Experimental materials were as-cast commercial AZ31 magnesium alloy which is composed of 3 wt.% Al, 1 wt.% Zn, 0.4 wt.% Mn and balance Mg. Materials were supplied by the YinGuang Magnesium industry group. The billet size was $\Phi 30$ mm \times 30 mm. Cast ingots were homogenized for 12 h at 420°C. Then, the AE processing was carried out at 350°C with an extrusion rate of 1 mm s⁻¹. The extrusion ratio was 11.11. Water-based graphite was used as a lubricant. In order to facilitate comparison, the same conditions of CE and AE are analyzed at the same time.

The microstructure of the as-cast, the CEed and the AEed samples were examined by OM and electron backscatter diffraction (EBSD) analysis. The

extrusion, transverse and normal directions of the extruded billet were defined as ED, TD and ND, respectively. The perpendicular to ED grain morphology was revealed by grinding and polishing processes and subsequently by etching using a solution of 1 ml acetic acid, 1 ml nitric acid, 1 g oxalic acid and 150 ml water. Tensile tests and EBSD experiments were done along the ED. Tensile samples were cylindrical with gauge length of $\Phi 3$ mm \times 15 mm and the experiments were carried out at room temperature with a strain rate of 1×10^{-3} s⁻¹. Each test was carried out at least five times, and the mechanical properties were the average values. The EBSD samples taken from the center of extruded products were ground using SiC papers and then electrolytically polished in an electrolyte solution which consisted of phosphoric acid and ethyl alcohol (volume ratio 3:5) at 0.5 A for 2 min and then at 0.2 A for 3 min. The EBSD tests were carried out by a 200°F Quanta field emission environmental scanning electron microscope, and the experimental data were analyzed by OIM Analysis TSL 6 software. The step size of EBSD measurements was 1.1 μ m.

The DEFORM 3D-6.1 software has been used to perform all deformation simulations. The simulations were conducted using an axisymmetric model. All objects dimensions in the simulation were matched with experimental ones in order to confirm the results of the simulation.¹⁷ The data of the true stress–strain based on the results of the compression test have been loaded into the finite element method (FEM) software. The material model was defined as elastic–plastic.¹⁸ All the die parts have been considered as rigid. The billet was defined as plastic, which can deform during all analyses. Tetrahedral element type was used, and the billet mesh number was 30,000. The Coulomb friction was used to model the interfaces between the die and the billet. The friction factor was selected as 0.8. The heat transfer coefficient between the die and the billet was N s⁻¹ mm⁻¹ °C⁻¹.¹⁹ The Lagrangian

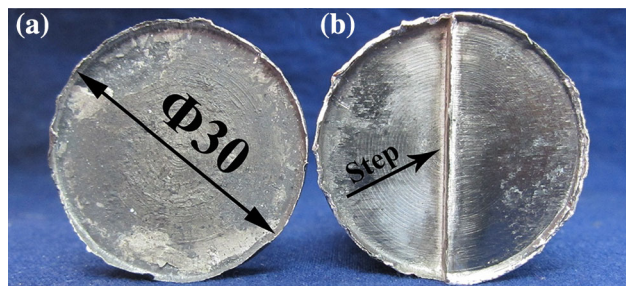


Fig. 2. The typical picture of extruded products: (a) CE at the end of process, (b) AE at the end of process.

incremental was chosen for the type of simulation. The conjugate gradient was chosen as the solver of the simulation. Axisymmetric four node elements were employed to model the billet sections.

RESULTS AND DISCUSSION

Figure 2 displays the CE and AE products. Compared with CE, there is an obvious step on the AE product. It seems that most of the materials such as aluminum, copper and magnesium and their alloys which can be processed via CE can also be processed by AE. It is promising that AE can be applied to a wide range of metallic materials but this statement needs experimental verification. The load of CE and AE obtained from FEM has been compared. Based on the obtained results, the required load of CE is equal to 133.8 kN, while the required load using AE is equal to 63.8 kN. Compared with CE, the total forming load of the AE process has been decreased by about 52%. This is an important advantage of AE.

Figure 3 shows the effective strain contours of the deformed billet during the CE and AE processes. To highlight the effective strain contours in the billet, the molds are not shown in the figures. For better observation of the effective strain distribution, the simulation results are presented in different color contour maps over the parallel (Fig. 3a and b) and vertical (Fig. 3c and d) cross-sections. Both CE and AE generate the maximum effective strain at the bottom die as shown in Fig. 3c and d. It can be seen that a shear deformation zone is generated during the AE process (Fig. 3b), which is different from the CE as shown in Fig. 3a. Therefore, AE can be divided into two distinct areas: the shear deformation zone and the normal strain zone. The shear deformation component plays an important role in grain refinement.²⁰ As shown in Fig. 3e, the effective strain in AE has been rapidly increased specifically near the middle area of the billet. The ten points selected to observe the effective strain are shown in Fig. 3a. To ensure the reliability and stability of the experimental results, ten points were also selected in the same position for AE. The maximum value of the effective strain was about 2.5 for AE, but only 0.03 for CE. This means that additional shear strain can be applied in AE

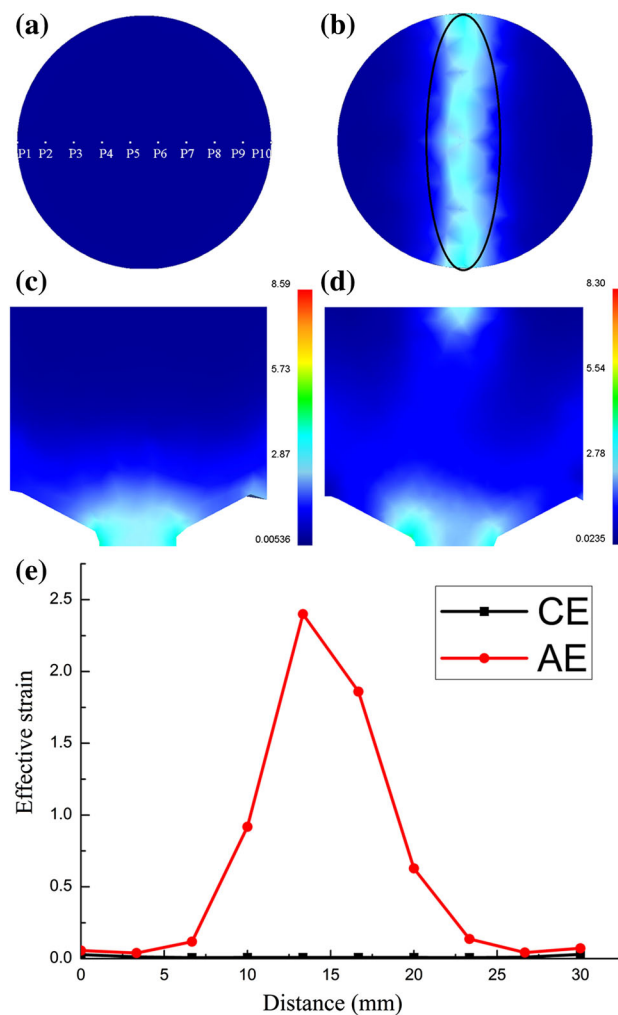


Fig. 3. Distribution of the effective strain for (a) CE parallel cross-sections, (b) AE parallel cross-sections, (c) CE vertical cross-sections, (d) AE vertical cross-sections, (e) the variation of the effective strain.

compared with CE. Generally, AE can bring the additional shear during the extrusion process, which indeed leads to further grain refinement. This is another advantage of AE.

Figure 4a–c illustrates a unique grain color map of the as-cast products and those processed with CE and AE. Different colors represent different grains rather than different orientations. To improve the accuracy of the results, the grains less than $4 \mu\text{m}$ are cleared and the grain tolerance angle is 5° . Figure 4d–f shows the grain structure perpendicular to the ED. According to statistical analysis of the grain size, the average grain size of the original billet is about $385 \mu\text{m}$. The original billet grains are coarse and uneven which will cause materials anisotropy and bad forming properties. After CE, the average grain size is $8.27 \mu\text{m}$. The standard deviation of the grain size after CE is $0.11 \mu\text{m}$. The morphology of grains has changed dramatically. Coarse grains are broken up and refined, but the

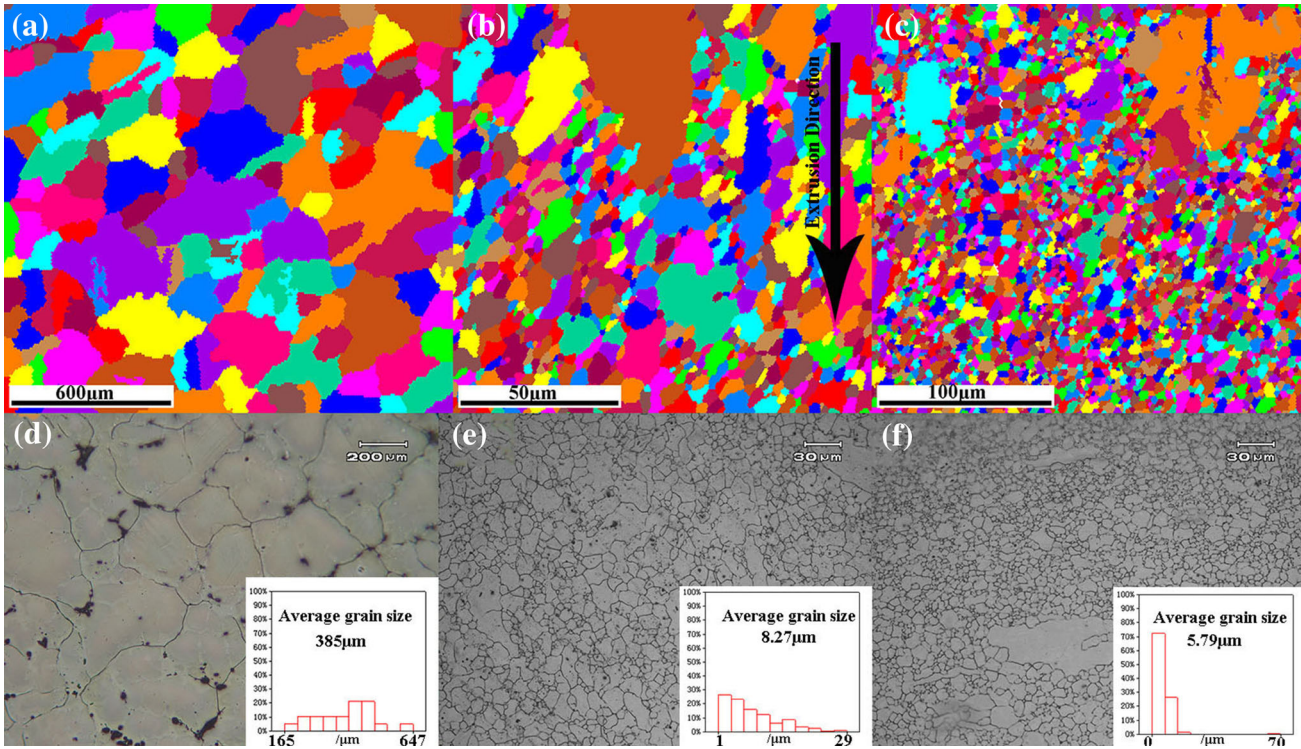


Fig. 4. The grain structure along ED: (a) original billet, (b) CEed products, (c) AEed products and perpendicular ED, (d) original billet, (e) CEed products, (f) AEed products.

distribution of grains is uneven. The banded structure which appears in the ED is clearly visible, and there are a lot of relatively small grains parallel to the ED. This indicates that the recrystallization occurred during the deformation.²¹ After AE, the grains are further refined and the average grain size reaches $5.79 \mu\text{m}$. The standard deviation of the grain size after AE is $0.21 \mu\text{m}$. AE can bring additional shear during the extrusion process, which provides a larger strain and has an effect on recrystallization. Therefore, the speed and rate of recrystallization are increased, bringing about an increasing number of refined grains. The number of the refined grains is beneficial to the improvement of the properties of AZ31 magnesium alloy.

Figure 5 shows the orientation maps and misorientation angles with different extrusion conditions. Figure 5a–c is the grain orientation image of the original billets, CE and AE, respectively. Each color on the maps indicates a crystallographic orientation. The red color represents the basal texture. It can be seen that the proportion of red decreases, indicating that the $\{0001\}$ planes gradually rotate in the AE process.

Figure 5d–f presents the misorientation angle distribution with different extrusion conditions. To ensure credible results, the misorientation angles less than 2° are not calculated. Most of the original billet grain boundaries are low-angle grain boundaries (LAGBs). The 2° – 15° misorientation angles account for 65% and the average misorientation

angle is 24° . After CE, the fraction of LAGBs decreases and the average misorientation angle reaches 65° . After AE, the 2° – 15° misorientation angles account for 27% and the average misorientation angle is 41° . Some studies have found that recrystallization grains often have high grain boundaries.^{22,23} Although the misorientation angles of CE and AE are larger than that of the original billet, low-angle grain boundaries still have a large part. Therefore, the products after CE and AE may experience an incomplete recrystallization.

Figure 6 shows the pole figures and inverse pole figures (IPF) in different extrusion conditions. Figure 6a shows that the basal plane texture of the original billet is scattered, indicating that there is a certain angle between the planes of the grain and the ED. After CE, the $\{0001\}$ basal plane of most grains are parallel to ED and texture intensity increases to 9.081, which demonstrates the formation of a typical $\{0001\}$ basal plane fiber extrusion texture via CE process. Compared with CE, the $\{0001\}$ basal plane is minimized after AE. Most grains' $\{0001\}$ basal planes are not parallel to ED, which is beneficial to activate the basal slip system.²⁴ On the whole, the texture is inclined to weaken after the AE process.

Figure 6b shows IPF pictures, which are perpendicular to the ND direction (an observation plane composed by TD and ED). After CE, the $\{0001\}$ basal plane of most grains is approximately parallel to the viewing plane. After AE, most of the grains have been rotated and pyramidal planes of $\{10\bar{1}3\}$ and

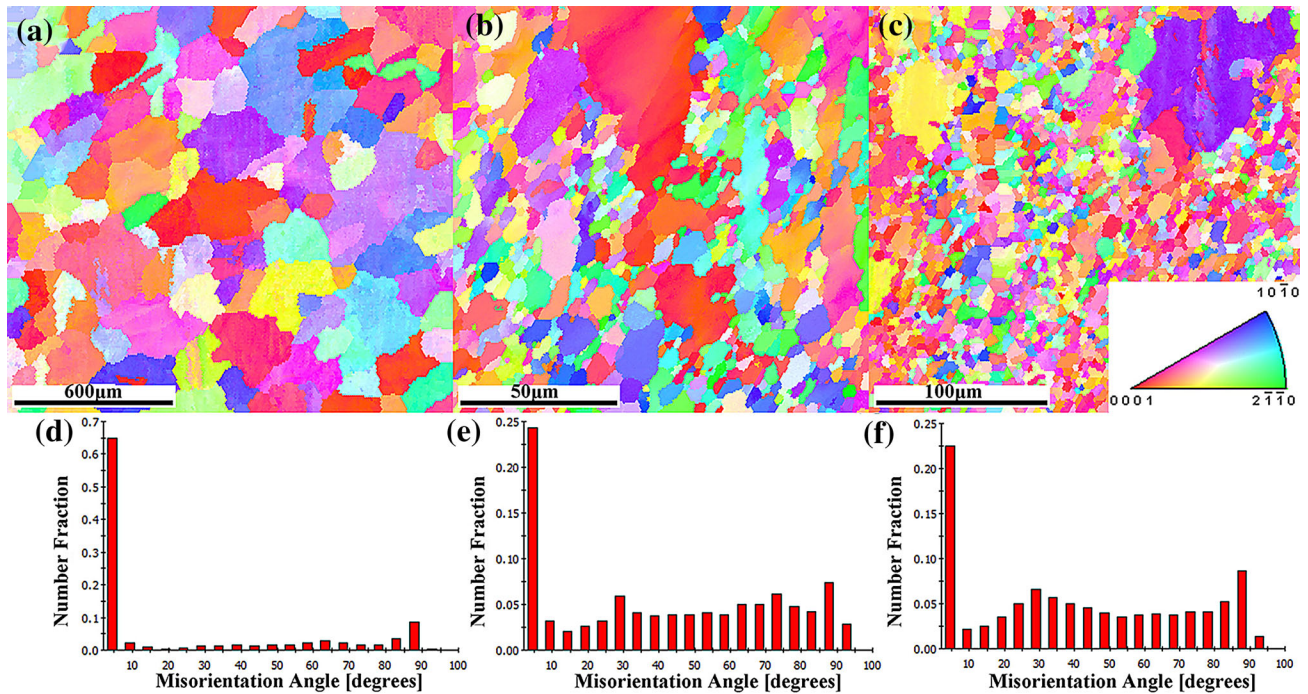


Fig. 5. The orientation maps of (a) original billet, (b) CE and (c) AE; the misorientation angle of (d) original billet, (e) CE and (f) AE.

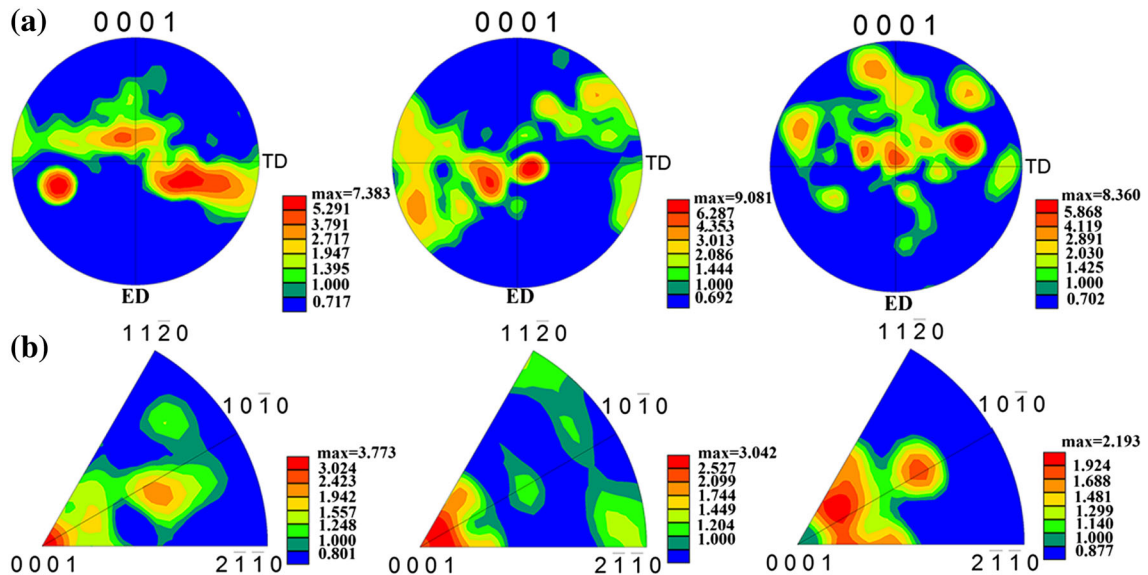


Fig. 6. Texture evolution under different extrusion conditions: (a) $\{0001\}$ pole figures, (b) IPF figures.

$\{10\bar{1}1\}$ are parallel to the observation plane. The intensities are: $\{10\bar{1}3\} > \{10\bar{1}1\}$. Type changes of texture and texture weakening are beneficial to reduce the anisotropy in the extrusion process of AZ31 magnesium alloy, which can obtain a uniform and stable plastic deformation and then improve the ability of plastic forming.²⁴

Figure 7 presents the average values of the tensile strength (TS), the 0.2% proof stress (YS) and the elongation. It can be found that the strength

and elongation are improved. Compared with CE, tensile strength increases from 271 MPa to 283 MPa, while elongation decreases from 13.8% to 12.5%. The standard deviation of the tensile strength after extrusion is 4.3 MPa and 7.8 MPa, respectively. Grain refinement and texture modification have been considered as effective methods to improve the mechanical properties of magnesium alloys. In addition to grain size and texture modification, the homogeneity microstructure also has a

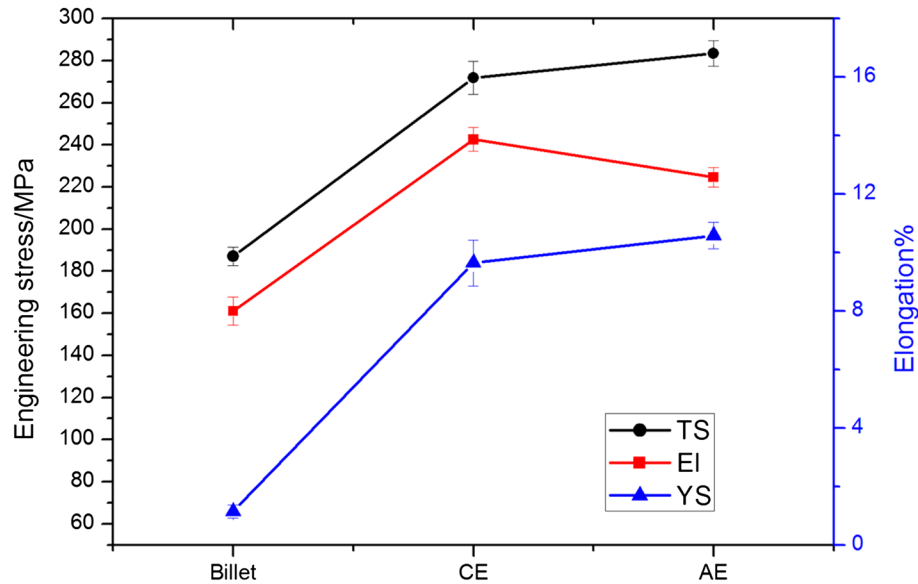


Fig. 7. The tensile properties of the billet, CE and AE at room temperature.

great influence on the mechanical properties of magnesium alloys at room temperature. The TS is mainly attributed to the average grain size. As can be seen in Fig. 4, the average grain size of the AE sample is smaller than those of the original and CE samples, which will result in high TS. It is noticed that the CE possesses relatively higher ductility than that of the AE samples. The reason for the elongation decrease of AE may be due to the fine brittle second-phase $Mg_{17}Al_{12}$ which causes some damage to the elongation. We have found an inhomogeneous microstructure of AE, which is the coexisting of very large grains and ultrafine grains in Fig. 4. Therefore, the unhomogeneous microstructure is also mainly ascribed to lower ductility. The research of Chang²⁵ revealed that the homogeneity of the microstructure played a significant role in the enhancement of ductility. Guo et al.²⁶ have found that the reduction in elongation after 1 pass repetitive upsetting (RU) is attributed to the inhomogeneous microstructure with the coexisting of very large grains and ultrafine grains. This special phenomenon will be further analyzed in subsequent studies.

CONCLUSION

An effective extrusion process called AE has been applied to fabricate an AZ31 magnesium alloy bar. The effective strain, microstructure characteristics and mechanical properties at room temperature are examined. The results are as follows:

1. Compared to the CE process, AE has a more excellent performance in refining the grain size.
2. The results show that the intensity of the basal plane texture is weakened and the samples fabricated using AE decline to form $\{10\bar{1}3\}$ and $\{10\bar{1}1\}$ pyramidal plane textures.

3. In the case of the similar mechanical properties of CE, the AE process provides a more economical extrusion method due to its lower extrusion load than the CE process.

ACKNOWLEDGEMENTS

This paper was financial project supported by National Natural Science Foundation of China (51205094) and Science Funds for the Young Innovative Talents of HUST, No. 2011.

REFERENCES

1. T.M. Pollock, *Science* 328, 986 (2010).
2. F.H. Froes, D. Eliezer, and E. Aghion, *JOM* 50(9), 30 (1998).
3. G.K. Meenashisundaram and M. Gupta, *JOM* 68(7), 1890 (2016).
4. M. Easton, A. Beer, M. Barnett, C. Davies, G. Dunlop, Y. Durandet, S. Blacket, T. Hilditch, and P. Beggs, *JOM* 60(11), 57 (2008).
5. Q. Chen, Z.X. Zhao, D.Y. Shu, D.Y. Shu, and Z.D. Zhao, *Mater. Sci. Eng. A* 528, 3930 (2011).
6. Q.S. Yang, B. Jiang, Y. Tian, W.J. Liu, and F.S. Pan, *Mater. Lett.* 100, 29 (2013).
7. F. Li, G.N. Chu, E.L. Liu, R.Z. Wu, and X.L. Zhang, *Proc. Inst. Mech. Eng. Part C J. Mech. Eng. Sci.* 225, 2927 (2011).
8. J. Stráská, M. Janeček, J. Čížek, J. Stráský, and B. Hadzima, *Mater. Charact.* 94, 69 (2014).
9. Z.X. Kang, L.L. Zhou, and J.Y. Zhang, *Mater. Sci. Eng. A* 633, 59 (2015).
10. E. Dogan, M.W. Vaughan, S.J. Wang, I. Karaman, and G. Proust, *Acta Mater.* 89, 408 (2015).
11. Y.J. Chen, Q.D. Wang, H.J. Roven, M.P. Liu, M. Karlsen, Y.D. Yu, and J. Hjelen, *Scr. Mater.* 58, 311 (2008).
12. S.M. Fatemi-Varzaneh, A. Zarei-Hanzaki, M. Naderi, and Ali.A. Roostaei, *J. Alloys Compd.* 507, 207 (2010).
13. S.H. Kim, B.S. You, C.D. Yim, and Y.M. Seo, *Mater. Lett.* 59, 3876 (2005).
14. K. Xia, J.T. Wang, X. Wu, G. Chen, and M. Gurvan, *Mater. Sci. Eng. A* 410–411, 324 (2005).
15. Q.D. Wang, Y.J. Chen, J.B. Lin, L.J. Zhang, and C.Q. Zhai, *Mater. Lett.* 61, 4599 (2007).

16. S.M. Fatemi-Varzaneh and A. Zarei-Hanzaki, *Mater. Sci. Eng. A* 528, 1334 (2011).
17. V. Shatermashhadi, B. Manafi, K. Abrinia, G. Faraji, and M. Sanei, *Mater. Des.* 62, 361 (2014).
18. P. Asadi, M.K.B. Givi, and M. Akbari, *Int. J. Adv. Manuf. Technol.* 83, 301 (2016).
19. F. Li, N. Bian, and Y.C. Xu, *Kovove Mater.* 53, 59 (2015).
20. D.H. Shin, I. Kim, J. Kim, and Y.T. Zhu, *Mater. Sci. Eng. A* 334, 239 (2002).
21. P.S. Roodposhti, A. Sarkar, and K.L. Murty, *Mater. Sci. Eng. A* 626, 195 (2015).
22. T. Al-Samman, X. Li, and S.G. Chowdhury, *Mater. Sci. Eng. A* 527, 3450 (2010).
23. J.A.D. Valle, M.T. Pérez-Prado, and O.A. Ruano, *Mater. Sci. Eng. A* 355, 68 (2003).
24. J. Bohlen, M.R. Nürnberg, J.W. Senn, D. Letzig, and S.R. Agnew, *Acta Mater.* 55, 2101 (2007).
25. L.L. Chang, J.H. Cho, and S.B. Kang, *J. Mater. Process. Technol.* 1527, 211 (2011).
26. W. Guo, Q.D. Wang, B. Ye, M.P. Liu, T. Peng, X.T. Liu, and H. Zhou, *Mater. Sci. Eng. A* 540, 115 (2012).